Original Research Article

International journal of spray and combustion dynamics

International Journal of Spray and Combustion Dynamics
2016, Vol. 8(4) 235–253

DOI: 10.1177/1756827716642091
scd.sagepub.com

SAGE

Dynamic data-driven prediction of instability in a swirl-stabilized combustor

Soumalya Sarkar[1,2], Satyanarayanan R Chakravarthy[3], Vikram Ramanan[3] and Asok Ray[1]

Abstract

Combustion instability poses a negative impact on the performance and structural durability of both land-based and aircraft gas turbine engines, and early detection of combustion instabilities is of paramount importance not only for performance monitoring and fault diagnosis, but also for initiating efficient decision and control of such engines. Combustion instability is, in general, characterized by self-sustained growth of large-amplitude pressure tones that are caused by a positive feedback arising from complex coupling of localized hydrodynamic perturbations, heat energy release, and acoustics of the combustor. This paper proposes a fast dynamic data-driven method for detecting early onsets of thermo-acoustic instabilities, where the underlying algorithms are built upon the concepts of symbolic time series analysis (STSA) via generalization of *D*-Markov machine construction. The proposed method captures the spatiotemporal co-dependence among time series from heterogeneous sensors (e.g. pressure and chemiluminescence) to generate an information-theoretic precursor, which is uniformly applicable across multiple operating regimes of the combustion process. The proposed method is experimentally validated on the time-series data, generated from a laboratory-scale swirl-stabilized combustor, while inducing thermo-acoustic instabilities for various protocols (e.g. increasing Reynolds number (*Re*) at a constant fuel flow rate and reducing equivalence ratio at a constant air flow rate) at varying air-fuel premixing levels. The underlying algorithms are developed based on *D*-Markov entropy rates, and the resulting instability precursor measure is rigorously compared with the state-of-the-art techniques in terms of its performance of instability prediction, computational complexity, and robustness to sensor noise.

Keywords

Gas turbine combustor, combustion instability, symbolic dynamics, probabilistic finite state automata, information theory

Date received: 1 September 2015; accepted: 1 March 2016

Introduction

Strict emission regulation has initiated a paradigm shift in the nominal operating conditions of gas turbine engines. Consequently, the technology of gas turbine engines has gradually adapted to low equivalence ratio combustion to suppress emissions of nitrogen oxides (NOx), instead of combustion at near-stoichiometric conditions. Ultra-lean premixed and pre-vaporized combustors, while being environment-friendly, are susceptible to combustion instability that is characterized by pressure waves with sharp tones and high amplitudes. The complexity of this instability problem accrues from the mutual interactions among the unsteady heat release rate, flow fields and acoustics, which outline the general features of combustion instability.[1–3] The prediction of combustion instability associated with swirl-stabilized flames is of particular interest in gas turbine combustion. The dynamics of three-dimensional swirl-stabilized flames are complex in nature as they are subjected to interactions of fluid-mechanical processes with the flame and acoustics,

[1]Department of Mechanical & Nuclear Engineering, Pennsylvania State University, University Park, PA, USA
[2]United Technology Research Center, East Hartford, CT, USA
[3]National Centre for Combustion R & D and Department of Aerospace Engineering, Indian Institute of Technology Madras, Chennai, India

Corresponding author:
Asok Ray, Department of Mechanical & Nuclear Engineering, Pennsylvania State University, University Park, Philadelphia, PA 16802, USA.
Email: axr2@psu.edu

which give rise to complex growth and saturation mechanisms. Reviews of swirl-stabilized flames and their instabilities have been reported by Huang and Yang[4] and Candel et al.[5] Significant studies in instabilities of swirl flames have also been conducted in the framework of flame transfer functions in the context of frequency-amplitude dependence and the underlying flow physics.[6,7] In particular, flame transfer functions provide low-order model-based tools that have been used to predict instabilities by solving the nonlinear dispersion relations as reported by Noiray et al.[8]

Full-scale computational-fluid-dynamic (CFD) models and/or reduced-order models have been developed to predict and characterize the combustion instabilities and specifically to identify the instability conditions; however, the underlying assumptions and inherent complexity in modeling the system dynamics as well as computational restrictions may result in imperfect validation by experimental observations. The other approach relies on time series data of physical sensors to identify the features that are capable of exclusively characterizing combustion instabilities. The resulting dynamic data-driven approach, based on time-series analysis, is less system-specific than the model-based approach as the former is more strongly dependent on the general features of various regimes in a combustor. In this regard, Nair and Sujith[9] have used the decay of Hurst exponents as precursors to detect impending combustion instabilities; other measures of instability like loss of chaotic behavior in the system dynamics have also been formulated.[10] The data-driven approach is, in general, expected to predict instabilities across the parameter space, within which the combustor operates. A key parameter is the inlet Reynolds number (*Re*), a variation of which has been observed to clearly mark the stable and unstable regimes of a combustor. Chakravarthy et al.[11] have reported the dawn of ''lock-on'', a term representing the frequency locking of natural duct acoustics and a dominant hydrodynamic mode as an essential feature of combustion instability. Specifically, ''lock-on'' is a generic feature and is independent of any geometric and fuel-based parameters. The hallmark feature of *Re* variations is the break in the dominant frequency, which corresponds to onset of combustion instability. Thus, the frequency break can be thought of as a reliable precursor for combustion instability. However, a major drawback is the bifurcation in the combustor behavior at the frequency break-point; therefore, it may not be used as a tool of early warning, thus motivating the need for a fast predictive tool that is generic. Both analytical and experimental investigations on the onset of thermo-acoustic instabilities have been reported by several researchers, for example, Lieuwen,[12] Gotoda et al.,[13,14] and Murugesan and Sujith.[15] Some of these recent studies have shown the possibility of encountering low-dimensional chaotic oscillations in combustors by employing several methods of nonlinear time series analysis. Recently, Nair et al.[16] have utilized recurrence quantization analysis (RQA) for prediction of instabilities, which detects a route of intermittency filled with random bursts of high amplitude oscillations.

The concept of symbolic time series analysis (STSA) has been used for anomaly detection in internal combustion engines by Daw et al.[17] as an extension of their earlier work[18] as well as by Mukhopadhyay et al.[19] and Unni et al.[20] for prediction of lean blowout and instability, respectively, in gas turbine combustors, which use the sensor data with little post-processing. The tools of STSA are further developed by Mukherjee and Ray[21] who have used an entropy-based method of state splitting and state merging as an extension of the earlier work of Ray and coworkers.[22–24] which requires a very modest amount of signal post-processing with the pay-off of a significantly enhanced capability for early prediction of the onset of anomalous behavior. Recently, Ramanan et al.[25] have used STSA with unity depth (memory) of the *D*-Markov machine to predict combustion instabilities from single sensor data for variations in *Re*. Along this line Sarkar et al.[26] have applied the notion of STSA with the generalized *D*-Markov machine construction (i.e. depth greater than one) to predict lean blow-out from chemiluminescence sensor time series for variations in equivalence ratio (Φ).

This paper proposes a fast STSA approach built upon the generalized *D*-Markov machine[21] to construct a complexity-based measure for detecting an early onset of thermo-acoustic instability in swirl-stabilized combustors. The proposed approach models spatio-temporal co-dependence among time series from heterogeneous (e.g. pressure and chemiluminescence) sensors to generate a data-driven precursor which is uniformly applicable across multiple experiment protocols with various premixing levels. From the perspectives of dynamic data-driven application systems (DDDAS) (e.g. see Darema[27] and references therein) and novel usage of STSA and *D*-Markov machine tools for analysis of combustion instability, major contributions of this paper are delineated below.

- Formulation of a robust measure of anomalous behavior in dynamical systems as a generalization of the D-Markov machine:[21,26] the objective is early prediction of combustion instability, which is robust to spurious disturbances.
- Development of an information-theoretic approach:[28] the underlying concept is built upon the entropy rates among heterogeneous sensors and

serves to construct alternative precursors for prediction of combustion instability.
- Experimental validation of the proposed concept of instability prediction: The test apparatus is a swirl-stabilized combustor, where thermo-acoustic instabilities are induced via different protocols (e.g. increasing Reynolds number (*Re*) at a constant fuel flow rate (FFR) and reducing equivalence ratio (Φ) at a constant air flow rate (AFR)) at varying levels of fuel premixing.
- Performance evaluation and comparison: The proposed instability precursor measure is compared with state-of-the-art techniques in terms of prediction performance (e.g. accuracy), computational complexity (i.e. memory requirement and execution time), and robustness to sensor noise.

The paper is organized in five sections, including the present one. "Description of the experimental apparatus" section describes the laboratory-scale swirl-stabilized combustor, which serves as a test apparatus for experimental validation of the proposed method of thermo-acoustic instability prediction. "STSA for instability prediction" section reviews the concept of STSA and presents extensions of STSA tools for modeling single time series and co-dependence among multiple time series. This section also formulates an anomaly measure for predicting combustion instability from single sensor and (possibly heterogeneous) multiple sensor data. "Results and discussion" section presents the capabilities and advantages of the proposed approach for instability prediction over different ranges of parameters and also provides a comparison with other state-of-the-art statistical measures for instability prediction. Finally, the paper is summarized and concluded in "Summary, conclusions and future work" section with selected recommendations for future research.

Description of the experimental apparatus

The experimental apparatus is built upon a laboratory-scale combustor (see Figure 1) that has a swirler of

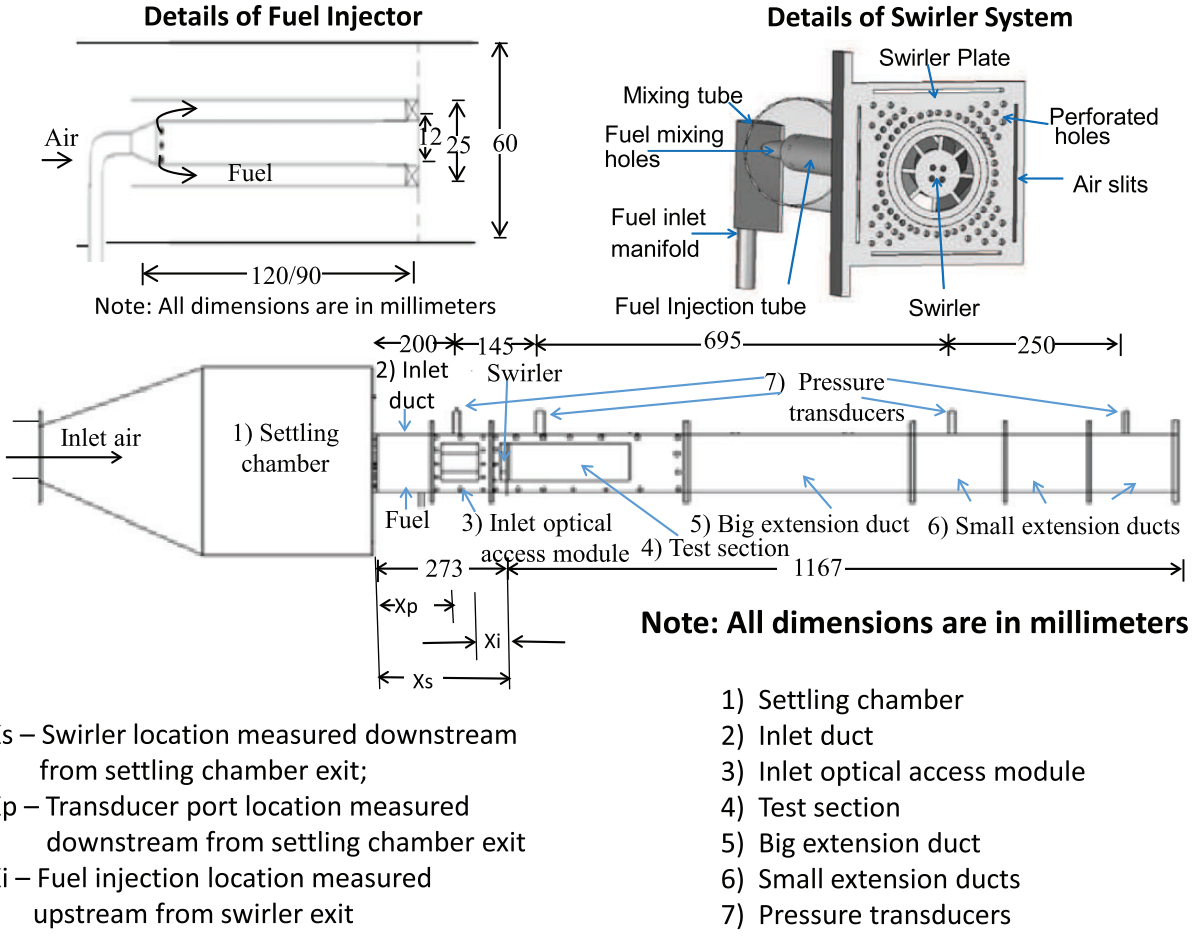

Figure 1. Schematic diagram of the laboratory-scale combustor apparatus.

diameter 30 mm with 60° vane angles, thus yielding a geometric swirl number of 1.28. Air to the combustor is fed through a settling chamber of diameter 280 mm with an abrupt contraction leading to a square cross section of side 60 mm. This provides an area ratio of around 17, which thus acts as an acoustically open condition at the contraction. A mesh and honeycomb are mounted in the immediate downstream of the contraction to provide uniform flow to the swirler. As seen in the schematic diagram of Figure 1, the combustor consists of the following major components: (i) an inlet section of length 200 mm; (ii) an inlet optical access module (IOAM) of length 100 mm to provide optical access to the fuel tube; (iii) a primary combustion chamber of length 370 mm, and a secondary duct of the same length; and (iv) extension ducts of the same cross section to provide length flexibility. The overall length of the constant area ducts is 1340 mm.

As shown in the top right hand corner of Figure 1, the fuel injection tube is coaxial to the mixing tube that has the same diameter as the swirler. The bypass air that does not enter the mixing tube passes through slots on the surface of swirl plate. The slots on the fuel injection tube are drilled at designated distances upstream of the swirler in different inserts; these are called upstream distances X_i corresponding to the designated location i of fuel injection. The larger is this distance, more fuel mixes with the primary air upstream in the mixing tube, thus leading to increased premixing. Two upstream distances of X_i, $1 = 1, 2$ have been used for the experimental work reported in this paper, where $X_1 = 90$ mm causes partial premixing of the fuel with air and is referred to as the partially premixed case, and $X_2 = 120$ mm provides better premixing of the fuel with the air and is referred to as the well premixed case. It has been observed from laboratory experiments that these fuel inlet positions yield sufficiently different premixing lengths, which are capable of classifying the resulting flames as well premixed and partially premixed. Exact quantification of the extent of premixing for fuel injection at these two locations is outside the scope of this paper and they are merely adopted as test cases to demonstrate the diversity of conditions under which the proposed STSA-based precursor prediction is validated.

In the experiments, 99.5% pure methane gas (CH_4) has been used as the fuel. Both air and FFRs are controlled by (Alicat Scientific make) mass flow controllers in the range of 0–4000 liters per minute (LPM) for air and 0–100 LPM for fuel.

Two major protocols have been followed in conducting the experiments.

- Protocol 1—Constant FFR, while varying the inlet air Re: the FFR is kept constant at 0.55 g/s for both the injection locations (i.e. $X_1 = 90$ mm and $X_2 = 120$ mm) for the constant FFR protocol, while the AFR is increased from $Re = 5300$, which corresponds to a starting global equivalence ratio of 1.59 and is varied in steps of 50 LPM till the onset of instability and subsequently 100 LPM after the onset till the flame blows out/off. A set of four wall-mounted (PCB make) piezo-electric pressure transducers are used, where the two most upstream transducers have sensitivity of 72 mV/kPa and the remaining two have sensitivity of 225 mV/kPa. The locations as well as normalized downstream distances from the inlet of these transducers are listed in Table 1. Spatially localized CH* chemiluminescence is measured by a wall-mounted photo-diode, equipped with a filter having 50 nm bandwidth and peak transmission at 430 nm, which is co-linear with the second transducer installed at the inlet.
- Protocol 2—Constant inlet Reynolds number (Re) while decreasing the FFR in the second protocol, three Re's are chosen as 8857, 10,630, and 12,400, while decreasing the FFR in very fine steps starting with an equivalence ratio of 0.955, till the flame blows out/off. Results are shown for $Re = 8857$. For this protocol, three piezo-electric pressure transducers (see Table 2) are used along the flow, which have a sensitivity of 225 mV/kPa.

Each of the data sets has been recorded for a time period of 3 s with all sensors synchronized at a sampling rate of 10 kHz via LabView signal express as the data acquisition system. High speed CH* chemiluminescence has been conducted to investigate the flame behavior at high and low amplitude conditions for operations under the protocols described above. The flame images have been acquired at 3 kHz using

Table 1. Locations of pressure transducers for the first protocol.

Transducer number	1	2	3	4
Distance from inlet end (mm)	200	345	1040	1290
Normalized distance	0.149	0.257	0.776	0.962

Table 2. Locations of pressure transducers for the second protocol.

Transducer number	1	2	3
Distance from inlet end (mm)	345	1040	1290
Normalized distance	0.257	0.776	0.962

Photron high speed star camera for a duration of 3 s and these images have been synchronized with data acquisition of unsteady pressure. A blue Kodak filter of bandwidth 50 nm and centered around 430 nm is mounted in front of the camera. The results shown subsequently pertain to $X_2 = 120$ mm and FFR of 0.495 g/s and *Re* of 15,942 for brevity. The results generated for other cases are reported in this paper for space limitations.

STSA for instability prediction

The chaotic behavior of the time series of pressure and chemiluminescence experiments at stable states of the combustion process includes transitions to high-amplitude ordered oscillations[9,10] at unstable states via routes of intermittency filled with random bursts of high-amplitude of oscillations.[16] It is conjectured that these phenomena are manifested by sharp changes in the time-series complexity. Furthermore, the temporal signals from multiple sensors, situated along the flow path, become aligned in phase at the instants of acoustic "lock-on",[11] which is a generic feature of thermo-acoustic instability. This section presents a computationally efficient tool, built upon the concepts of STSA and information theory (e.g. entropy and mutual information[29]), which is capable of capturing small changes in both complexity and inter-sensor co-dependence for early detection of the onset of instability phenomena.

Tools of STSA are built upon the concept of symbolic dynamics,[30] which deals with discretization of dynamical systems in both space and time. The notion of STSA has led to the development of a (nonlinear) data-driven feature extraction tool for dynamical systems. Figure 2 schematically presents a flow chart that explains how the STSA tool symbolizes multi-sensor signals via partitioning to construct *D*-Markov machines and $\times D$-Markov machines for modeling single sensor time series. The concept of *D*-Markov machines leads to the construction of $\times D$-Markov machines based on the cross relationship between heterogeneous (e.g. pressure and chemiluminescence) signals. This is followed by computation of entropy-based measures to detect combustion instabilities at an early stage. The individual modules of STSA, as seen in Figure 2, and the formulation of entropy-based instability measure are described as follows.

In STSA, a time series of sensor signals is represented as a symbol sequence that, in turn, leads to the construction of probabilistic finite state automata (PFSA).[31,32] Since PFSA models are capable of efficiently compressing the information embedded in the sensor time series,[22,21] these models could enhance the performance and execution speed of information fusion and information source localization that are often computation-intensive. Rao et al.[33] and Bahrampour et al.[34] have shown that the performance of this PFSA-based tool as a feature extractor for statistical pattern recognition is comparable (and often superior) to that of other

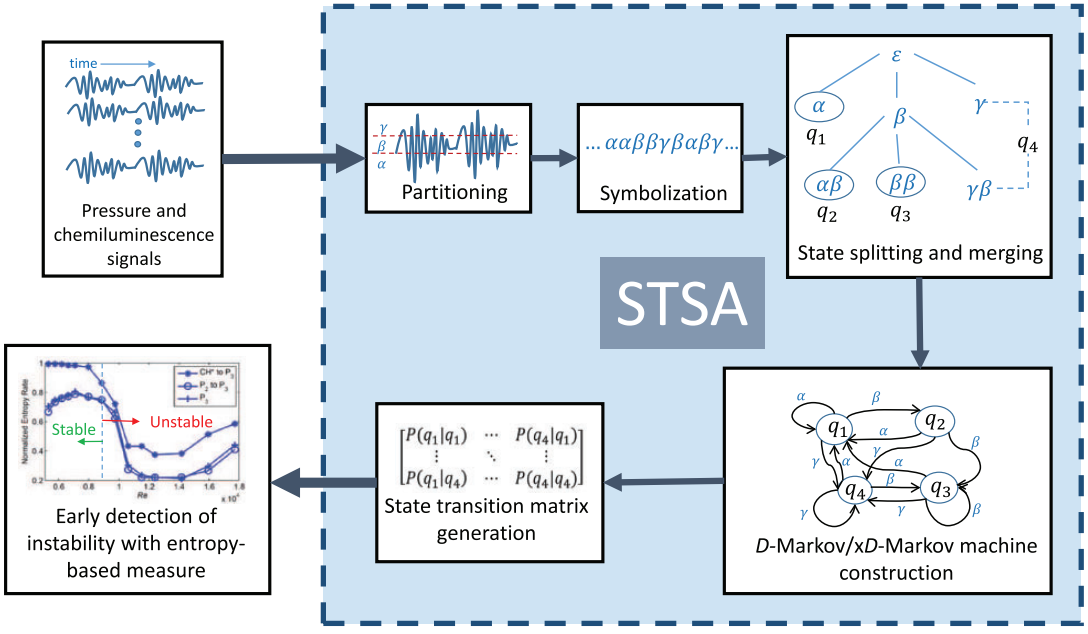

Figure 2. The schematics of symbolic time series analysis (STSA) for early detection of combustion instability via entropy based measure.

existing techniques (e.g. Bayesian filters, artificial neural networks, and principal component analysis[35]).

The signal space of time series is partitioned into finitely many mutually exclusive and exhaustive cells for symbolization, where each cell corresponds to a single symbol belonging to a (finite) alphabet Σ. As a trajectory of the dynamical system passes through or touches various cells of the partition, the symbol assigned to the cell is inserted in the symbol string. In this way, a time series corresponding to a trajectory is converted into a symbol string. Figure 2 illustrates the concept of constructing finite state automata (FSA) from time series, which provides the algebraic structure of PFSA. There are different types of partitioning tools, such as maximum entropy partitioning (MEP) and uniform partitioning (UP).[23] This paper has adopted MEP for symbolization of time series, which maximizes the entropy of the generated symbols by putting (approximately) equal number of data points in each partition cell; consequently, the information-rich regions of a time-series are partitioned finer and those with sparse information are partitioned coarser.

The next step is to construct PFSA from the symbol strings to encode the embedded statistical information so that the dynamical system's behavior is captured by the patterns generated from the PFSA in a compact form. The algebraic structure of PFSA (i.e. the underlying FSA) consists of a finite set of states that are interconnected by transitions,[36] where each transition corresponds to a symbol in the (finite) alphabet. At each step, the automaton moves from one state to another (including self loops) via these transitions, and thus generates a corresponding block of symbols, so that the probability distributions over the set of all possible strings defined over the alphabet are represented in the space of PFSA as stated below.

Definition 3.1. (PFSA) A PFSA is constructed on the algebraic structure of deterministic finite state automata (DFSA) $G = (\Sigma, Q, \delta)$ as a pair $K = (G, \pi)$, i.e. the PFSA K is a 4-tuple $K = (\Sigma, Q, \delta, \pi)$, where:

1. Σ is a non-empty finite set, called the symbol alphabet, with cardinality $|\Sigma| > \infty$;
2. Q is a non-empty finite set, called the set of states, with cardinality $|Q| > \infty$;
3. $\delta : Q \times \Sigma \to Q$ is the state transition map;
4. $\pi : Q \times \Sigma \to [0, 1]$ is the symbol generation function (also called probability morph function) that satisfies the condition $\sum_{\sigma \in \Sigma} \pi(q, \sigma) = 1 \quad \forall q \in Q$, and π_{ij} is the probability of emission of a symbol $\sigma_j \in \Sigma$ when the state $q_i \in Q$ is observed.

The advantage of such a representation is that the PFSA structure is simple enough to be encoded as it is characterized by the set of states, the transitions (i.e. exactly one transition for each symbol generated at a state), and the transition's probability of occurrence.

The D-Markov machine

This subsection presents the underlying concept of D-Markov machines[22,21] as models of probabilistic languages based on the algebraic structure of PFSA. In D-Markov machines, the future symbol is causally dependent on the (most recently generated) finite set of (at most) D symbols, where D is a positive integer. The underlying FSA in the PFSA of D-Markov machines are deterministic, i.e. the future state is a deterministic function of the current state and the observed symbol. Therefore, D-Markov machines essentially encode two entities: (1) probability of generating a symbol at a given state, and (2) deterministic evolution of future states from the current state and the symbol. A D-Markov machine is formally defined as:

Definition 3.2. (D-Markov) A D-Markov machine is a statistically stationary stochastic process $S = \cdots s_{-1} s_0 s_1 \cdots$ (modeled by a PFSA in which each state is represented by a finite history of at most D symbols), where the probability of occurrence of a new symbol depends only on the last D symbols, i.e.

$$P[s_n | \cdots s_{n-D} \cdots s_{n-1}] = P[s_n | s_{n-D} \cdots s_{n-1}] \tag{1}$$

- D is called the depth of the Markov machine;
- Q is the finite set of states with cardinality $|Q| \leq |\Sigma|^D$, i.e. the states are represented by equivalence classes of symbol strings of maximum length D, where each symbol belongs to the alphabet Σ;
- $\delta : Q \times \Sigma \to Q$ is the state transition function that satisfies the following condition: if $|Q| = |\Sigma|^D$, then there exist $\alpha, \beta \in \Sigma$ and $x \in \Sigma^\star$ such that $\delta(\alpha x, \beta) = x\beta$ and $\alpha x, x\beta \in Q$.

The complexity of a D-Markov machine is reflected by the entropy rate which also represents its overall capability of prediction. The entropy rate of a D-Markov machine is defined as:

Definition 3.3. (D-Markov entropy rate) The D-Markov entropy rate of a PFSA (Σ, Q, δ, π) is defined in terms of the conditional entropy as:

$$\begin{aligned} H(\Sigma|Q) &\triangleq \sum_{q \in Q} P(q) H(\Sigma|q) \\ &= -\sum_{q \in Q} \sum_{\sigma \in \Sigma} P(q) P(\sigma|q) \log P(\sigma|q) \end{aligned} \tag{2}$$

where $P(q)$ is the probability of a PFSA state $q \in Q$ and $P(\sigma|q)$ is the conditional probability of a symbol $\sigma \in \Sigma$ given that a PFSA state $q \in Q$ is observed.

Construction of a D-Markov machine

The underlying procedure for construction of a D-Markov machine[21] from a symbol sequence consists of two major steps: state splitting and state merging.[21,26] In general, state splitting increases the number of states to achieve more precision in representing the information content in the time series. State splitting effectively reduces the entropy rate $H(\Sigma|Q)$, thereby focusing on the critical states (i.e. those states that carry more information).

The subsequent process of state merging reduces the number of states in the D-Markov machine by merging those states that have similar statistical behavior. Thus, a combination of state splitting and state merging leads to the final form of the D-Markov machine as described below.

State splitting. The number of states of a D-Markov machine of depth D is bounded above by $|\Sigma|^D$, where $|\Sigma|$ is the cardinality of the alphabet Σ. As this relation is exponential in nature, the number of states rapidly increases as D is increased. However, from the perspective of modeling a symbol sequence, some states may be more important than others in terms of their embedded information contents. Therefore, it is advantageous to have a set of states that correspond to symbol blocks of different lengths. This is accomplished by starting off with the simplest set of states (i.e. $Q = \Sigma$ for $D = 1$) and subsequently splitting the current state that results in the largest decrease of the D-Markov entropy rate.

The process of splitting a state $q \in Q$ is executed by replacing the symbol block q by its branches as described by the set $\{\sigma q : \sigma \in \Sigma\}$ of words. Figure 3 illustrates the process of state splitting in a PFSA with alphabet $\Sigma = \{0, 1\}$, where each terminal state is circumscribed by an ellipse. Let $q \in Q$ be a state of a D-Markov machine (see Definition 3.2), which is split to yield new states σq, where $\sigma \in \Sigma$ and σq represents the equivalence class of all (finite-length) symbol strings with the word σq as the suffix. For example in Figure 3, the states in the third layer from the top are: $00q, 10q, 01q$, and $11q$, of which all but $10q$ are terminal states. Consequently, the state $10q$ is further split as: $010q$ and $110q$ that are also terminal states, i.e. $Q = \{00q, 01q, 11q, 010q, 110q\}$. The operation of state splitting along with the algorithm is described in more detail in Mukherjee and Ray.[21]

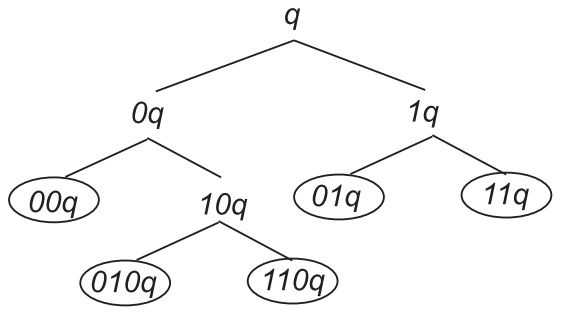

Figure 3. Tree-representation of state splitting in D-Markov machines.

Maximum reduction of the entropy rate is the governing criterion for selecting the state to be split. In addition, the generated set of states must satisfy the self-consistency criterion, which only permits a unique transition to emanate from a state for a given symbol. If $\delta(q, \sigma)$ is not unique for each $\sigma \in \Sigma$, then the state q is split further. In the state splitting algorithm, a stopping rule is constructed by specifying the threshold parameter η_{spl} on the rate of decrease of conditional entropy. An alternative stopping rule for the algorithm is to provide a maximal number of states $N_{\max}$ instead of the threshold parameter η_{spl}.

For construction of PFSA, each element $\pi(\sigma, q)$ of the morph matrix Π is estimated by frequency counting as the ratio of the number of times, $N(q\sigma)$, the state q is followed (i.e. suffixed) by the symbol σ and the number of times, $N(q)$, the state q occurs; the details are available in Mukherjee and Ray.[21] The estimated morph matrix $\hat{\Pi}$ is obtained as:

$$\hat{\pi}(q, \sigma) \triangleq \frac{1 + N(q\sigma)}{|\Sigma| + N(q)} \ \forall \sigma \in \Sigma \ \forall q \in Q \tag{3}$$

where $\sum_{\sigma \in \Sigma} \hat{\pi}(\sigma, q) = 1 \ \forall q \in Q$. Similarly, the stationary state probability vector is estimated by frequency counting as:

$$\hat{P}(q) \triangleq \frac{1 + N(q)}{|Q| + \sum_{q' \in Q} N(q')} \ \forall q \in Q \tag{4}$$

where $\hat{P}(q)$ is an element of the estimated stationary state probability vector, i.e. probability of the PFSA being in the state $q \in Q$. Then, the D-Markov entropy rate (see Definition 3.3) is computed as:

$$\begin{aligned} H(\Sigma|Q) &= -\sum_{q \in Q} \sum_{\sigma \in \Sigma} P(q) P(\sigma|q) \log P(\sigma|q) \\ &\approx -\sum_{q \in Q} \sum_{\sigma \in \Sigma} \hat{P}(q) \hat{\pi}(q, \sigma) \log \hat{\pi}(q, \sigma) \end{aligned} \tag{5}$$

State merging. The motivation for state merging is to reduce the number of states, while preserving the

sufficient D-Markov structure of a PFSA. Nevertheless, such a process may cause the PFSA to have degraded precision due to loss of information. The state merging algorithm aims to mitigate this risk via a stopping rule that is constructed by specifying an acceptable threshold η_{mrg} on the distance $\Psi(\cdot,\cdot)$ between the merged PFSA and the PFSA generated from the original time series. The distance metric $\Psi(\cdot,\cdot)$ is defined as:

Definition 3.4. (Distance Metric between two PFSAs). Let $K_1 = (\Sigma, Q_1, \delta_1, \pi_1)$ and $K_2 = (\Sigma, Q_2, \delta_2, \pi_2)$ be two PFSA with a common alphabet Σ. Let $P_1(\Sigma^j)$ and $P_2(\Sigma^j)$ be the steady state probability vectors of generating words of length j from the PFSA K_1 and K_2, respectively, i.e. $P_1(\Sigma^j) \triangleq [P(w)]_{w\in\Sigma^j}$ for K_1 and $P_2(\Sigma^j) \triangleq [P(w)]_{w\in\Sigma^j}$ for K_2. Then, the metric for the distance between the PFSA K_1 and K_2 is defined as

$$\Psi(K_1, K_2) \triangleq \lim_{n\to\infty} \sum_{j=1}^{n} \frac{\left\| P_1(\Sigma^j) - P_2(\Sigma^j) \right\|_{\ell_1}}{2^{j+1}} \tag{6}$$

where the norm $\|\star\|_{\ell_1}$ indicates the sum of absolute values of the elements in the vector $\star$.

States that behave similarly (i.e. have similar morph probabilities) have a higher priority for merging. The similarity of two states, $q, q' \in Q$, is measured in terms of the respective morph functions of future symbol generation as the distance between the two rows of the estimated morph matrix $\hat{\Pi}$ corresponding to the states q and q'. The ℓ_1-norm (i.e. the sum of absolute values of the vector components) has been adopted to be the distance function as seen below.

$$\begin{aligned} \mathcal{M}(q, q') &\triangleq \left\| \hat{\pi}(q, \cdot) - \hat{\pi}(q', \cdot) \right\|_{\ell_1} \\ &= \sum_{\sigma\in\Sigma} |\hat{\pi}(q, \sigma) - \hat{\pi}(q', \sigma)| \end{aligned} \tag{7}$$

A small value of $\mathcal{M}(q, q')$ indicates that the two states have close probabilities of generating each symbol. Hence, the two closest states (i.e. the pair of states $q, q' \in Q$ having the smallest value of $\mathcal{M}(q, q')$) are merged using the merging algorithm explained in Mukherjee and Ray.[21] The merging algorithm updates the morph matrix and transition function in such a way that does not permit any ambiguity of nondeterminism.[22] Subsequently, distance $\Psi(\cdot,\cdot)$ of the merged PFSA from the initial symbol string is evaluated. If $\Psi > \eta_{\text{mrg}}$ where η_{mrg} is a specified threshold, then the machine structure is retained and the states next on the priority list are merged. On the other hand, if $\Psi \geq \eta_{\text{mrg}}$, then the process of merging the given pair of states is aborted and another pair of states with the next smallest value of $\mathcal{M}(q, q')$ is selected for merging. This procedure is terminated if no such pair of states exist, for which $\Psi > \eta_{\text{mrg}}$.

The $\times$D-Markov machine

In the setting of a PFSA (e.g. D-Markov machine), a $\times$ D-Markov machine[37] captures the statistical co-dependence between two (synchronized) time-series after symbolization. A symbol block of (finite) length D in a symbol sequence $\{\mathbf{s}_1\}$ may affect the subsequent symbols observed in another symbol sequence $\{\mathbf{s}_2\}$ and vice versa. In this setting, the $\times D$-Markov machine is formally defined as:

Definition 3.5. ($\times D$-Markov) Let the symbol sequences $\{\mathbf{s}_1\}$ and $\{\mathbf{s}_2\}$ generate PFSAs (e.g. D-Markov machines) K_1 and K_2, respectively (see Definition 3.1 and Definition 3.2). Then, a $\times D$-Markov machine from $\{\mathbf{s}_1\}$ to $\{\mathbf{s}_2\}$ is defined as a 5-tuple $K_{1\to2} \triangleq (\mathcal{Q}_1, \Sigma_1, \Sigma_2, \delta_1, \Pi_{12})$ such that:

- $\mathcal{Q}_1 = \{q_1, \ldots, q_{|>rm>\mathcal{Q}_1|}\}$ is the state set corresponding to symbol sequence $\{\mathbf{s}_1\}$.
- $\Sigma_1 = \{\sigma_0, \ldots, \sigma_{|\Sigma_1|-1}\}$ is the alphabet set of symbol sequence $\{\mathbf{s}_1\}$.
- $\Sigma_2 = \{\sigma_0, \ldots, \sigma_{|\Sigma_2|-1}\}$ is the alphabet set of symbol sequence $\{\mathbf{s}_2\}$.
- $\delta_1 : \mathcal{Q}_1 \times \Sigma_1 \to \mathcal{Q}_1$ is the state transition mapping for K_1.
- Π_{12} is the $(|\mathcal{Q}_1| \times |\Sigma_2|)$ cross-morph matrix and its ijth element $(\pi_{12}(q_{1i}, \sigma_{2j}))$ denotes the probability of finding the symbol σ_{2j} in the symbol sequence $\{\mathbf{s}_2\}$ at the next time step while making a transition from the state q_{1i} of the PFSA constructed from the symbol sequence $\{\mathbf{s}_1\}$.

Similarly, a 5-tuple $\times D$-Markov machine $K_{2\to1} \triangleq (\mathcal{Q}_2, \Sigma_2, \Sigma_1, \delta_2, \Pi_{21})$ is constructed from symbol sequences $\{\mathbf{s}_2\}$ to $\{\mathbf{s}_1\}$.

Similar to D-Markov entropy rate (see Definition 3.3), $\times D$-Markov entropy rate is formally defined as:

Definition 3.6. ($\times D$-Markov entropy rate[37]) $\times D$-Markov entropy rate from a PFSA $(\Sigma_1, Q_1, \delta_1, \pi_1)$ to a symbol sequence $\{\mathbf{s}_2\}$ in alphabet Σ_2 is defined as:

$$\begin{aligned} H(\Sigma_2|Q_1) &\triangleq \sum_{q_1\in Q_1} P(q_1) H(\Sigma_2|q_1) \\ &= -\sum_{q_1\in Q_1} \sum_{\sigma_2\in\Sigma_2} P(q_1) P(\sigma_2|q_1) \log P(\sigma_2|q_1) \end{aligned} \tag{8}$$

where $P(q_1)$ is the probability of a PFSA state $q_1 \in Q_1$ and $P(\sigma_2|q_1)$ is the probability of a symbol $\sigma_2 \in \Sigma_2$ given that a PFSA state $q_1 \in Q_1$ is observed.

Remark 3.1. The $\times D$-Markov entropy rate represents the overall predictability of a symbol sequence when a PFSA from another symbol sequence is observed. It is a measure of the dynamical complexity of the temporal codependence from one symbol sequence to another. As an example related to combustion physics, a slight shift from stable combustion toward thermo-acoustic instability can be captured by an abrupt increase in the computed value of $\times D$-Markov entropy rate.

Construction of a $\times$D-Markov machine

Similar to the construction of a D-Markov machine,[37] a major challenge in the construction of a $\times D$-Markov machine is the trade-off between modeling accuracy and model order that is major source of computational complexity (i.e. execution time and memory requirements). Optimal models for $\times D$-Markov machines are generated by an information-theoretic approach that relies on the D-Markov and $\times D$-Markov entropy rates (see Definitions 3.3 and 3.6). These entropy rates are computed from the time series of individual sensor data (e.g. pressure and chemiluminescence).

Figure 4 illustrates the underlying procedure of state splitting in the construction of a $\times D$-Markov machine. The process of splitting a state $q_1 \in Q_1$ is executed by replacing the symbol block q_1 by its branches as described by the set $\{\sigma_1 q_1 : \sigma_1 \in \Sigma_1\}$ of words in the symbol sequence $\{\mathbf{s}_1\}$. Maximum reduction of the $\times D$-Markov entropy rate is the governing criterion for selecting the state to be split. In addition, the generated set of states must satisfy the self-consistency criterion[21] for the PFSA K_1, which implies a unique transition to emanate from a state for a given symbol. Similar to state splitting in D-Markov machines, a stopping rule for state splitting is constructed either by specifying a threshold parameter η_{spl} on the rate of decrease of $\times D$-Markov entropy rate or by providing a maximal number of states $N_{\max}$ of PFSA K_1.

At each step of state splitting, each element $\pi_{12}(\sigma_2, q_1)$ of the cross morph matrix Π_{12} is estimated by frequency counting as the ratio of the number of times, $N(q_1\sigma_2)$, the state q_1 from $\{\mathbf{s}_1\}$ is followed by the symbol σ_2 from $\{\mathbf{s}_2\}$ and the number of times, $N(q_1)$, the state q_1 occurs. Each element $\hat{\pi}_{12}(q_1, \sigma_2)$ of the estimated morph matrix $\hat{\Pi}_{12}$ is obtained as:

$$\hat{\pi}_{12}(q_1, \sigma_2) \triangleq \frac{1 + N(q_1\sigma_2)}{|\Sigma_2| + N(q_1)} \quad \forall \sigma_2 \in \Sigma_2 \; \forall q_1 \in Q_1 \tag{9}$$

where $\sum_{\sigma_2 \in \Sigma_2} \hat{\pi}_{12}(\sigma_2, q_1) = 1 \; \forall q_1 \in Q_1$. Similar to equation (9), each element $P(q_1)$ of the stationary state probability vector for the PFSA from $\{\mathbf{s}_1\}$ at a splitting stage is estimated by frequency counting as:

$$\hat{P}(q_1) \triangleq \frac{1 + N(q_1)}{|Q_1| + \sum\limits_{q_1' \in Q_1} N(q_1')} \quad \forall q_1 \in Q_1 \tag{10}$$

where $\hat{P}(q_1)$ is the estimated stationary probability of the PFSA being in the state $q_1 \in Q_1$. The $\times D$-Markov entropy rate (see equation (8)) is computed in terms of the state probability vector for the PFSA, generated from the symbol sequence $\{\mathbf{s}_1\}$, and estimated cross morph matrix as:

$$\begin{aligned} H(\Sigma_2|Q_1) &= -\sum_{q_1 \in Q_1} \sum_{\sigma_2 \in \Sigma_2} P(q_1) P(\sigma_2|q_1) \log P(\sigma_2|q_1) \\ &\approx -\sum_{q_1 \in Q_1} \sum_{\sigma_2 \in \Sigma_2} \hat{P}(q_1) \hat{\pi}_{12}(q_1, \sigma_2) \log \hat{\pi}_{12}(q_1, \sigma_2) \end{aligned} \tag{11}$$

Based on the specific threshold, the process of state splitting is continued till the optimal $\times D$-Markov machine is constructed. The estimated morph matrix $\hat{\Pi}_{12}$, in its final form, is used as a representative feature of the causality from the first to the second time-series.

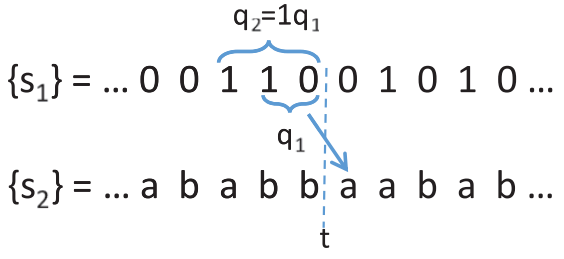

Figure 4. Variable depth xD-Markov machine.

Results and discussion

This section presents the results of analysis of pressure and chemiluminescence sensor data, generated from the experimental apparatus (see "Description of the experimental apparatus" section). This section also evaluates the performance of the proposed method for prediction of combustion instability by comparison with state-of-the-art techniques.

Preliminary analysis of acquired data

The swirl combustor's stability behavior is first analyzed by fast Fourier transform (FFT) to estimate the spectral contents of the signals generated in the operational regime. The results are shown in Figure 5, where the individual plots correspond to the transducer recordings of highest amplitudes and spectral values at different values of the Reynolds number (Re).

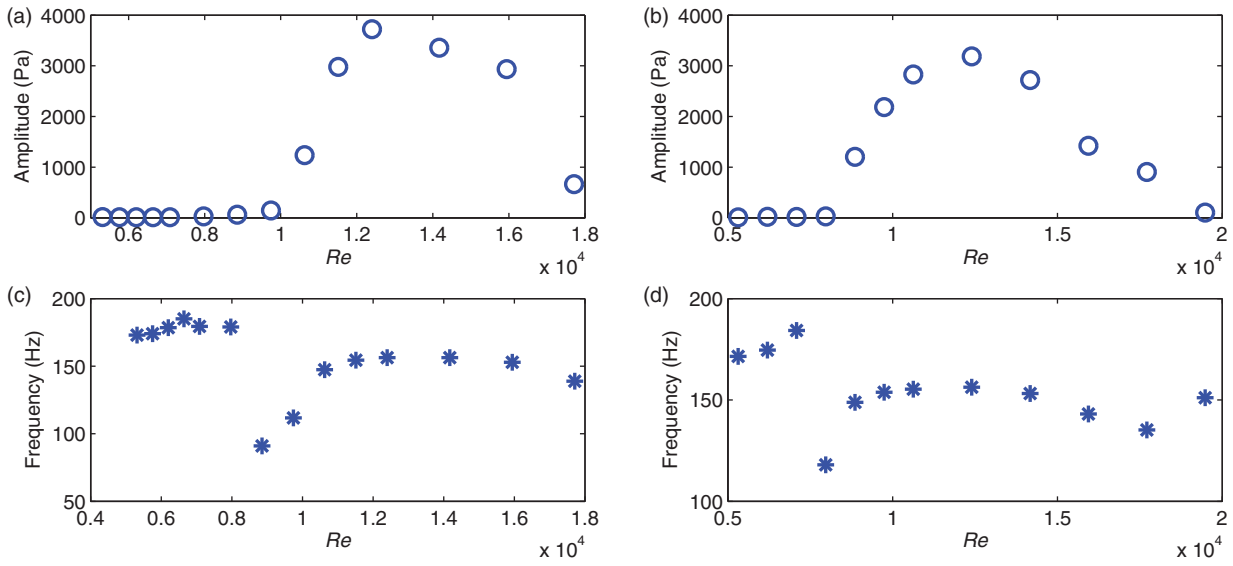

Figure 5. Unsteady pressure characteristics (i.e. amplitude and frequency) at constant fuel flow rate (FFR) of 0.55 mg/s for (a), (c) partially premixed and (b), (d) well premixed fuel.

It is seen in Figure 5 that the combustor system may exhibit a sharp change (i.e. increase or decrease) in acoustic pressure characteristics as *Re* is varied and thus poses a challenge for instability prediction. It is also evident that, independent of the upstream distance of fuel injection (see "Description of the experimental apparatus" section), the rise in the spectral amplitude is slightly preceded by a break in the dominant frequency, similar to the observations made by Chakravarthy et al.[11] The nature of the combustion instability during these transitions also shows that the dominant frequency closely scales with *Re*. It is seen for both partially premixed ($X_1 = 90$ mm) and well premixed ($X_2 = 120$ mm) cases that, during a transition to instability (e.g. in the vicinity of $Re = 9000$ for partial premixing), there exists an approximately linearly increasing dominant frequency. This frequency signifies an excited hydrodynamically coherent structure that drives the transition to combustion instability, followed by an almost constant-frequency trend that implies frequency-locking of all drivers of combustion instability.

Figure 6 exhibits the combustor behavior at a constant value of *Re* by varying the global equivalence ratio Φ. For $Re = 8857$, the combustor behavior for both partially premixed and well premixed cases is similar to that for constant FFR in the sense that the combustor abruptly becomes unstable at a lower Φ along with a discontinuity in the profile of dominant frequency. For the cases investigated in this paper, a break in the dominant frequency can be treated as a defining feature to indicate the onset of combustion instability. This phenomenon can be explained in terms of the phase difference between the unsteady heat release rate and the pressure wave approaching each other and thus possibly rendering a frequency mode unstable. The combustor is found to be stable at the either ends of the operational regime, with the flame extinction occurring at very low pressure amplitudes. This is in contrast to the partially premixed flame for a constant FFR, where the pressure amplitudes are high and thus acoustics could play a major role in the flame extinction. Investigation of this behavior is a topic of future research as delineated in "Summary, conclusions and future work" section.

Variation of state complexity

Figure 7 shows that, for different experiment protocols (see "Description of the experimental apparatus" section), the cardinality of the state space drops drastically at the onset of instability and again rises when the system becomes relatively stable or reaches lean blowout. Furthermore, the usage of MEP for symbol generation in the PFSA model construction (see "STSA for instability prediction" section) can be justified because of the observed equi-distribution of squared intensity across all modes except the mean flame mode. The presence of a large number of states seen in stable combustion can be ascribed to a large number of modes having the same squared intensity values, which may make omission of states difficult and unreasonable. This may warrant usage of a large number of states, which individually contribute very negligibly to the overall flame mode. Since the second and third modes dominate the signal characteristics for unstable combustion,

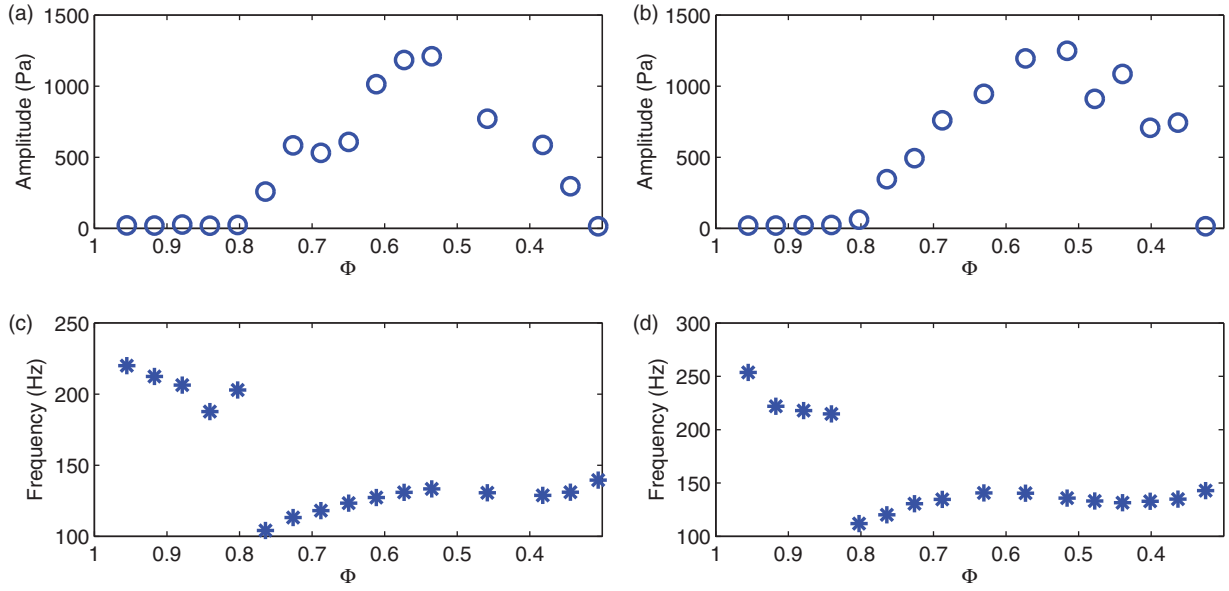

Figure 6. Amplitude and frequency of unsteady pressure at constant Reynolds number (Re) = 8857: left column (a), (c) partially premixed; right column (b), (d) well premixed fuel.

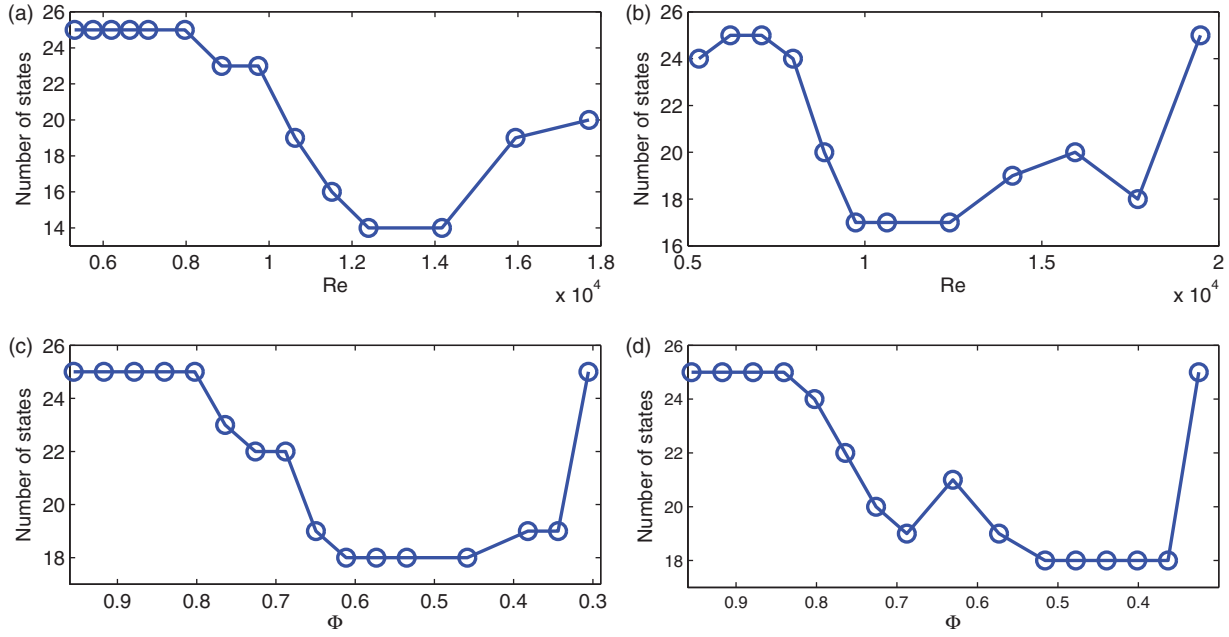

Figure 7. Variation of state space cardinality $|Q|$ of dominant pressure time series with increasing Re (D-Markov construction with alphabet size $\Sigma = 5$ and splitting threshold for maximal number of states $N_{max} = 25$) at constant fuel flow rate (FFR) of 0.55 mg/s for (a) partially premixed ($X_i = 90$ mm) and (b) well premixed fuel ($X_i = 120$ mm) conditions; similar variation with decreasing equivalence ratio Φ at constant Re of 8857 for (c) partially premixed ($X_i = 90$ mm) and (d) well premixed fuel ($X_i = 120$ mm) conditions.

the total number of significant states is just two, after eliminating the mean flame mode; this is far less than the number of states used to describe stable combustion. The state complexity derived through STSA corroborates the same.

Instability prediction by D-Markov and ×D-Markov entropy rates

At each condition for different protocols, sets of time series data from pressure and chemiluminescence

sensors have been collected over intervals of 3 s at 10 kHz sampling frequency. To reduce the occurrence of self loops in the state transition matrix and to increase the efficacy of texture identification via D-Markov and $\times D$-Markov machine construction, each time series is downsampled by a factor of 10 (i.e. effective sampling interval of 1 ms) based on the first occurrence of minimal mutual information of individual time series,[38] which is similar to finding the embedding delay in nonlinear time-series analysis.[39]

Although modeling of PFSA (e.g. D-Markov machines) from symbol sequences has been widely reported, similar efforts have not been expended to investigate how to find an appropriate alphabet size for partitioning the underlying time series so that the symbol sequences can be optimally generated. Sarkar et al.[40] have addressed this critical issue in the context of pattern classification and proposed an information-theoretic procedure of data partitioning to extract low-dimensional features from time series. The key idea lies in optimal partitioning of the time series via maximization of the mutual information between the state probability vector of PFSA and the members of the pattern classes. However, in practice, the optimal alphabet size is often reduced to enhance computational efficiency, especially for fast processes like combustion dynamics. In this paper, an alphabet size of $|\Sigma| = 3$ is selected for symbolization of time series for all sensors at each condition, which is smaller than the derived optimal $|\Sigma|$ that were found to be approximately in the range of 4–6 for different time series data. It has been observed from the analyses of various time series of experimental data that the performance (i.e. decisions of instability prediction) is not significantly affected due to this carefully determined reduction of the alphabet size in individual cases, while there is a huge gain in computation time and memory. The rationale is that a larger alphabet size causes a larger set of PFSA states that give rise to larger matrices to be handled by the real-time algorithm.

Upon selection of the alphabet size, each time series is symbolized by MEP to construct D-Markov machines and $\times D$-Markov machines. For example, D-Markov machines are constructed from the respective dominant pressure time series and $\times D$-Markov machines are constructed to capture the variations of co-dependence between pairs of sensor time series data as described in "STSA for instability prediction" section. For state splitting,[21] the parameter $\eta_{\text{spl}} = 0.01$ is chosen as the stopping criterion and the state space is constructed from 25% of the ensemble of time series. Both D-Markov and $\times D$-Markov entropies are computed by making use of the remaining 75%.

The first row of Figure 8((a) partially premixed and (b) well premixed fuel conditions) shows variations in the *rms* value, P_{rms}, of pressure of the most dominant pressure sensor (P_3) with increasing Re at constant FFR = 0.55 mg/s. The second row of Figure 8 shows the profiles of D-Markov and $\times D$-Markov entropy rates with increasing Re in the similar order as the first row. It is observed that the $\times D$-Markov entropy rate directed from the chemiluminescence sensor (CH*) to P_3 drops with a slope that is significantly larger than the increasing slope of P_{rms} of pressure. This particular characteristic of $\times D$-Markov entropy rate captures both phase synchronization among sensors (along the abscissa Re) due to acoustic "lock-on" and loss of chaos (e.g. limit cycle stabilization) in the combustion process at the onset of instability. The $\times D$-Markov entropy rate from P_2 to P_3 and D-Markov entropy rate of P_3 behave similarly as they are situated close to each other at the combustor. Entropy rates attain small values in the instability regime as the dynamical complexity of the data is low for large amplitude periodic oscillations. Apparently, the entropy rates start to increase again before the occurrence of flame blowout; it is observed that the blowout occurs at lower entropy rates in the partially premixed condition than that in the well premixed condition. This is corroborated by higher acoustic amplitudes at blowout for this case than in the well premixed case, noted earlier. By using a suitable threshold on entropy rates (e.g. $\times D$-Markov entropy rate directed from CH* to P_3), instability can be predicted earlier than P_{rms} prediction with a smaller probability of false alarms.

Figure 9 presents the characteristics of P_{rms} and D-Markov and $\times D$-Markov entropy rates in a similar way as in Figure 8, but with the exception that the equivalence ratio Φ is reduced at a constant Re of 8857 and the AFR remains unchanged. It is observed that both entropy rates decrease at a faster rate at the onset of instability for well premixed condition than that for partially premixed condition. Both entropy rates perform well as a predictor of instability, especially, for well premixed condition, as the number of precursor events (i.e. intermittence phenomenon) is higher. For both premixing conditions, combustion blowout occurs at a high entropy rate which implies that the system has regained the original chaotic behavior from the significantly more ordered oscillations during instability.

Robustness of the $\times D$-Markov entropy rates as an instability measure has been examined with respect to the data length of time series. Figure 10 shows that the $\times D$-Markov entropy rate from the chemiluminescence sensor to P_3 varies as a function of Re within a tight bound for data over time periods ranging from 0.5 s to 3 s. A possible reason for relatively larger variations in $\times D$-Markov entropy rates (for different data lengths at $Re = 8857$) is the presence of intermittent bursts of high amplitude oscillation causing the onset of instability.

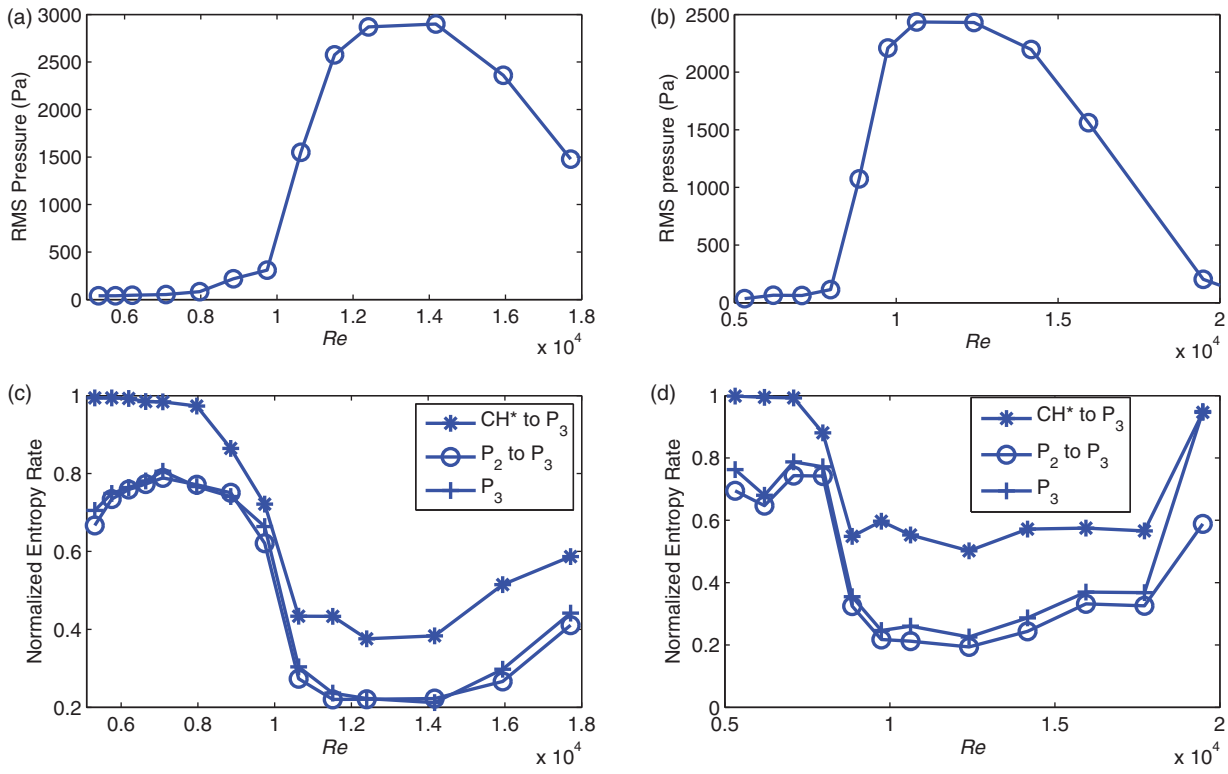

Figure 8. For a constant fuel flow rate (FFR) of 0.55 mg/s and with increasing *Re*, changes in the *rms* value (P_{rms}) of the most dominant pressure sensor (P_3) at (a) partially premixed and (b) well premixed fuel conditions. Variations of *D*-Markov entropy rates of time series from P_3, $\times D$-Markov entropy rates obtained from the $\times D$-Markov machine directed from P_2 (upstream of P_3) to P_3, and from the chemiluminescence sensor (CH^* upstream of P_3) to P_3 at (c) partially premixed and (d) well premixed fuel conditions.

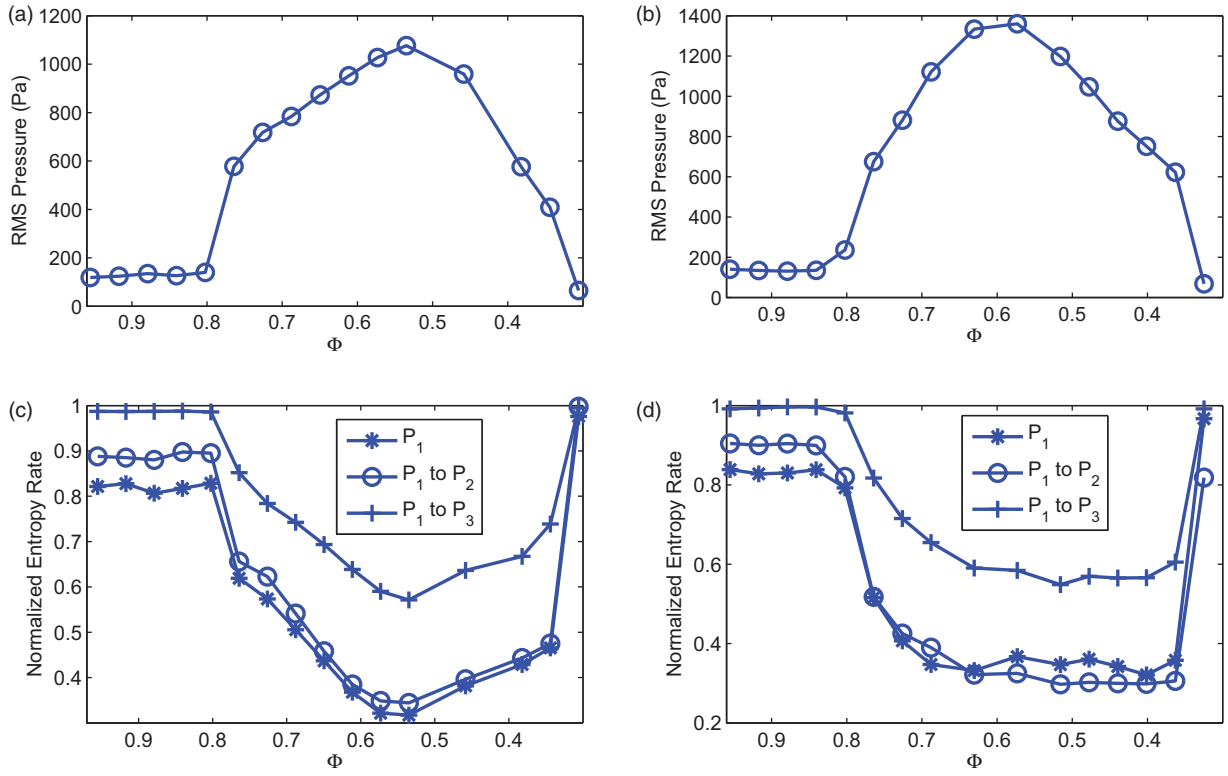

Figure 9. For a constant Reynolds number *Re* of 8857 (and unchanged AFR) and with decreasing equivalence ratio Φ, changes in the *rms* value (Pa) of pressure of the dominant pressure sensor (P_1) at (a) partially premixed and (b) well premixed fuel conditions. Variations of *D*-Markov entropy rates of time series from P_1, $\times D$-Markov entropy rates from the $\times D$-Markov machine directed from P_1 to P_2 (downstream of P_1) and from P_1 to P_3 at (c) partially premixed and (d) well premixed fuel conditions.

Comparison with other state-of-the-art techniques

Multiple competing methods have been recently proposed in the domain of data-driven instability prediction. For example, Gotoda et al.[14] have observed variations of minimum permutation entropy[41] as a function of equivalence ratio Φ to detect the degree of complexity of pressure time series at the onset of combustion instability. They have also observed that the dynamic behavior in combustion instability near lean blowout exhibits a self-affine structure, which is ascribed to fractional Brownian motion and undergoes chaos by the onset of combustion oscillations with slow amplitude modulation. Nair and Sujith[9] have proposed decay of generalized Hurst exponent to show the loss of multifractal nature of combustion pressure time series at the onset of instability, where a threshold of 0.1 has been used for early prediction of instability. Nair et al.[16] have proposed another instability prediction technique based on RQA that identifies the route of intermittency punctuated with random bursts of high amplitude oscillations. All these methods have been validated on limited scenarios of premixing conditions and protocols. Unni and Sujith[42] have presented a multifractal description for lean blowout in combustors with turbulent flow based on a unified framework within which both thermo-acoustic instability and blowout can be described.

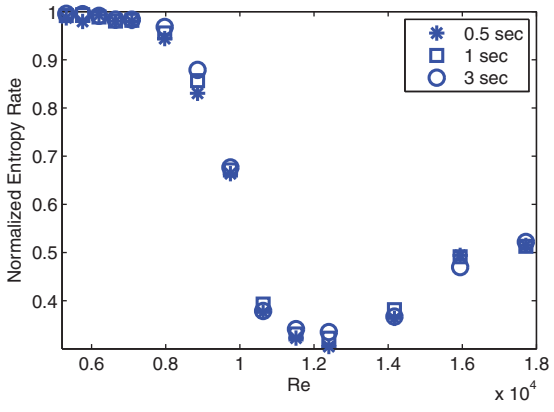

Figure 10. For constant fuel flow rate (FFR) of 0.55 mg/s and with increasing *Re*, variation of x*D*-Markov entropy rates obtained from the x*D*-Markov machine directed from the chemiluminescence sensor (*CH**, upstream to P_3) to P_3 at partially premixed condition for different data lengths.

Computational complexity. The processing time of the aforementioned techniques is compared with that of the proposed $\times D$-Markov entropy rate as a function of the time-series length. The comparison is carried out in the MATLAB-2014 environment on a computation platform of Dell Precision T3400 PC with Intel(R) Core(TM) 2 Quad CPU Q9550 @ 2.83 GHz 2.83 GHz. The recurrence rate (RR)[16] is computed to serve as an instability measure from the pressure time series; this information is embedded nonlinearly within a 10-dimensional space. Before constructing the recurrence plot, the signal is downsampled corresponding to a sampling frequency of 2.5 kHz that is identified via Taken's theorem[38,39] with a time delay of 1 ms. The threshold for calculating the RR is chosen to be slightly higher than the size of the attractor obtained at the lowest operational Reynolds number (*Re*)[16] in each of the experimentation protocols (see "Description of the experimental apparatus" section). It is observed that the time complexity of this method increases approximately quadratically with data length (i.e. $O(n^2)$ with the data length of n).

Figure 11(a) presents the processing time for calculating minimum permutation entropy[14] from pressure

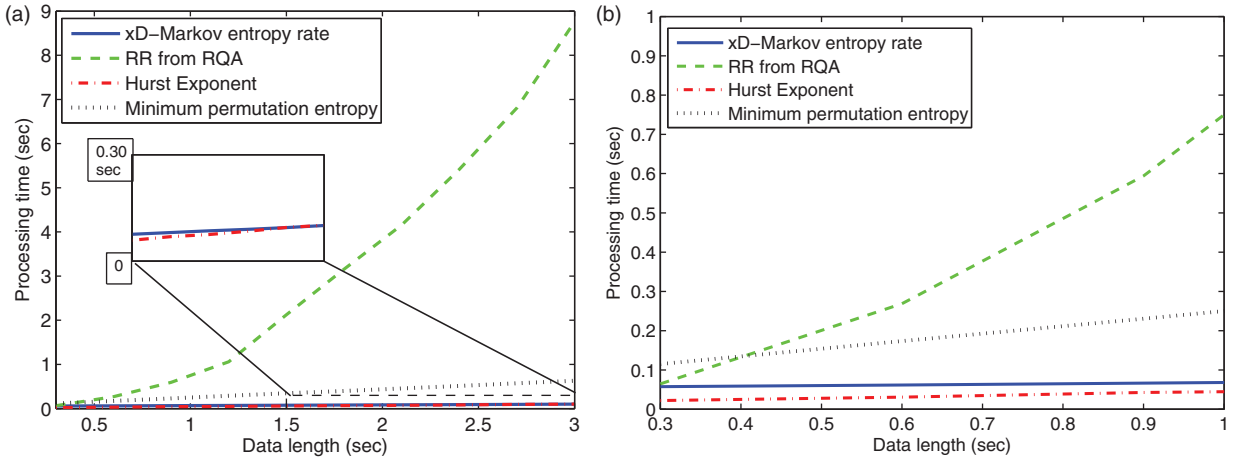

Figure 11. Time complexity of different methods for early prediction of combustion instability: (a) data collected over time periods varying from 0.3 s to 3 s; and (b) zoomed-in version where the data is from 0.3 s to 1 s.

time series, which varies linearly with data length. The minimum permutation entropy is obtained by (multiple times with varying order) usage of a fast window-based algorithm[43] on pressure data that are downsampled to 5 kHz with an embedding delay of 1 ms similar to Gotoda et al.[14] The time complexity for computation of both Hurst exponent[9] and ×D-Markov entropy rate (see Instability prediction by D-Markov and $\times D$-Markov entropy rates subsection) vary linearly with data length and have very small slopes. The mean of the Hurst exponent of order 2 is estimated here with a range of time scales ranging from 15 ms to 30 ms (i.e. 2–4 full cycles). It takes around ~ 100 ms to calculate $\times D$-Markov entropy rate from a 3-s (i.e. 30,000 long) time series, which is slightly larger than that of Hurst exponent; such a small computational time makes the method potentially suitable for real-time combustion control. Figure 11(b) shows a zoomed-in portion of Figure 11(a) to highlight the fact that, for short data over ~ 0.3 s, the processing time of different methods appears to be comparable; however, they tend to diverge as the data length is increased by a small amount. The processing time for ×D-Markov entropy rate can be reduced substantially from the presented value if these models can be generated offline at different operating conditions.

Performance evaluation. As seen in Figure 11, the time complexities of Hurst exponent and $\times D$-Markov entropy rate are comparable. Figure 12 presents variations of Hurst exponent and $\times D$-Markov entropy rate as a function of Re at the partially premixed condition ($X_1 = 90$ mm) for constant FFR of 0.55 mg/s. It is observed that $\times D$-Markov entropy rate demonstrates a monotonic nature starting at unity as Re is varied from stability to instability unlike the Hurst exponent which is fluctuating before the onset of instability. If a threshold of 0.9 is applied on $\times D$-Markov entropy rate, it detects the onset of instability as early as Hurst exponent does with a threshold of 0.1.[9] Figure 13 presents the variation of Hurst exponent and $\times D$-Markov entropy rate as a function of Φ at partially premixed condition ($X_1 = 90$ mm) for constant Re of 8857. It is apparent from the characteristics of the Hurst exponent

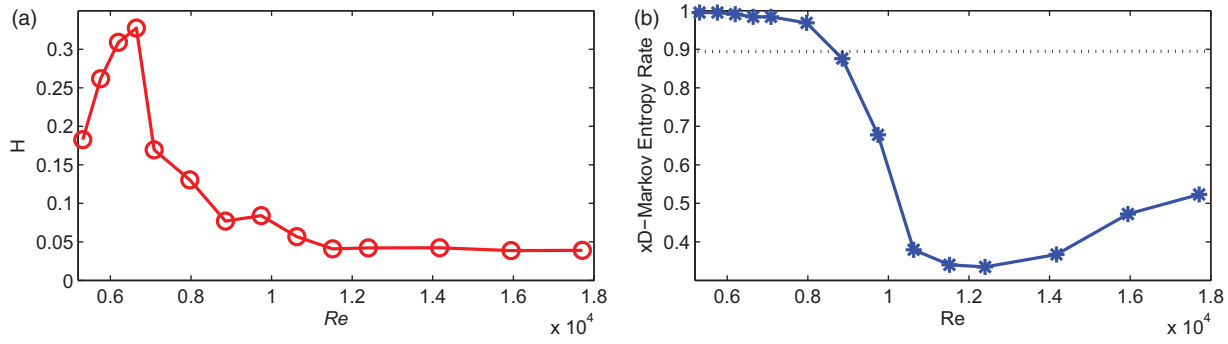

Figure 12. For constant fuel flow rate (FFR) of 0.55 mg/s and with increasing Re, (a) variation of Hurst exponent for the dominant pressure sensor P_3 and (b) variation of $\times D$-Markov entropy rates obtained from the chemiluminescence sensor (CH^*, upstream to P_3) to P_3 at partially premixed condition; the threshold is set at 0.9 for early detection of onset of instability.

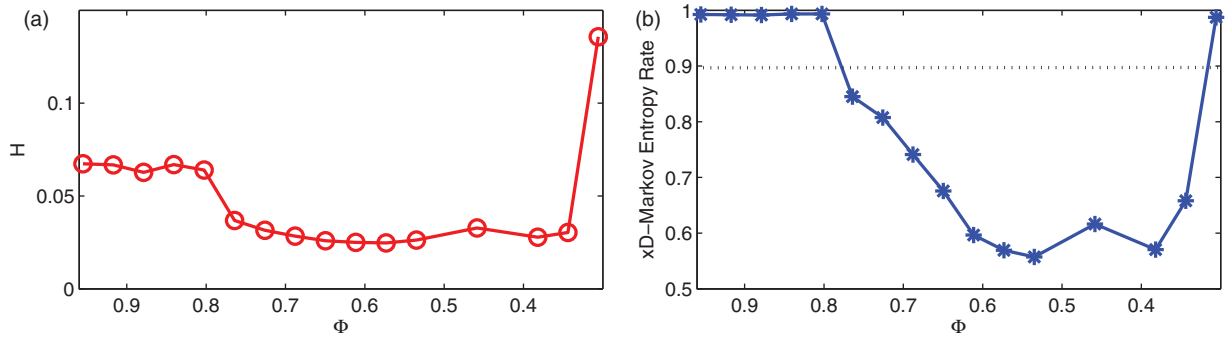

Figure 13. For constant Re of 8857 (unchanged air flow rate) and with decreasing equivalence ratio Φ, (a) variation of Hurst exponent for the dominant pressure sensor P_1 and (b) variation of $\times D$-Markov entropy rates from P_1 to P_3 (downstream of P_1) at partially premixed condition; the threshold is set at 0.9 for early detection of onset of instability.

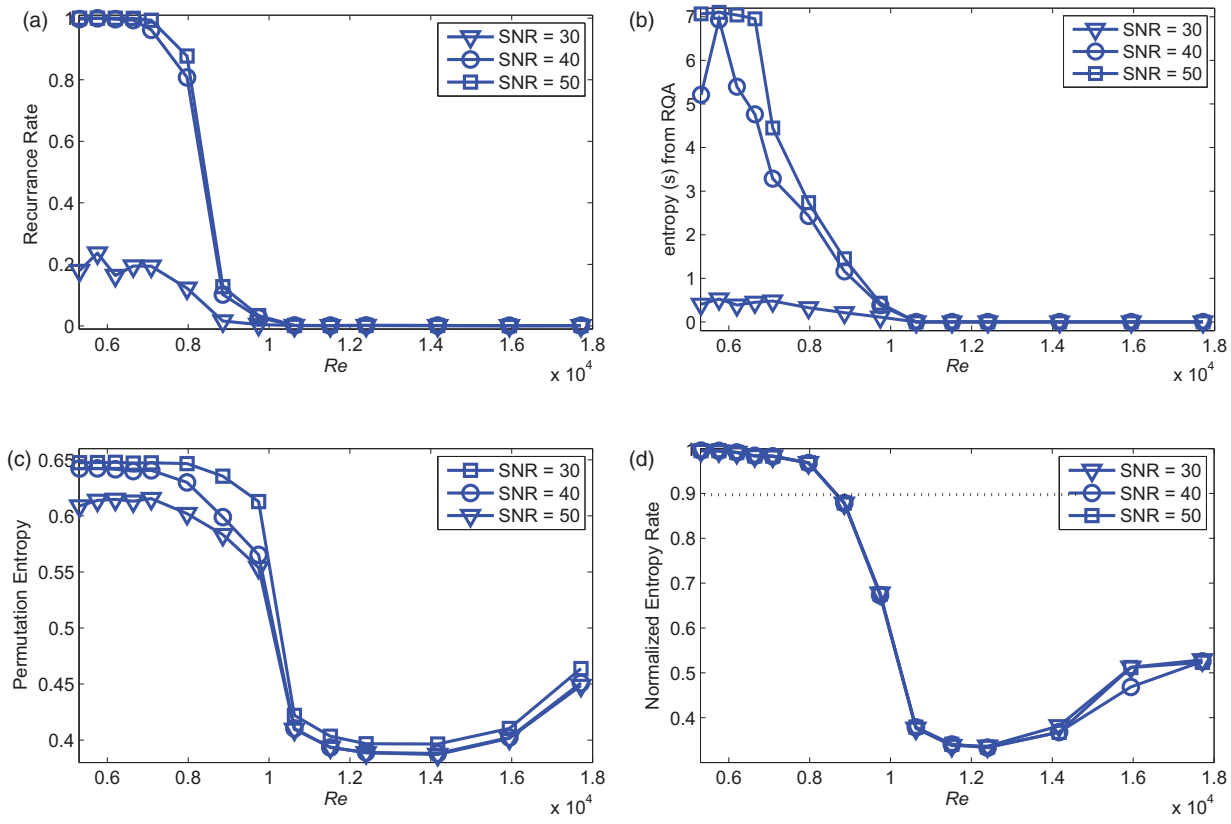

Figure 14. For constant fuel flow rate (FFR) of 0.55 mg/s and with increasing *Re*, variation of (a) the recurrence rate (RR) of pressure time traces (P_3) at 2.5 kHz for 3 s, which measures the density of points in the recurrence plot; (b) the entropy (s) of the diagonal length distribution; (c) the minimum permutation entropy of P_3; (d) $\times D$-Markov entropy rates obtained from the chemiluminescence sensor (*CH**, upstream to P_3) to P_3 at partially premixed condition (threshold is set at 0.9 for early detection of onset of instability) for different sensor noise levels (SNR = 30, 40 and 50 dB w.r.t. 0 dBW signal).

that the threshold parameter should be changed from 0.1 to some value around 0.05 to reduce the probability of false alarms. For $\times D$-Markov entropy rate from P_1 to P_3 (which is farthest downstream of P_1), the threshold of 0.9 at constant FFR can be applied for early detection of onset of instability. With this same threshold for different premixing levels, $\times D$-Markov entropy rate is capable of detecting an onset of instability with similar slopes for changes in parameters (e.g. *Re* and Φ) as RR obtained by the RQA method[16] and with superior performance than that from the minimum permutation entropy method.[14]

Robustness to sensor noise. This subsection compares the robustness of different statistical measures for instability prediction to different level of sensor noise along with the proposed measure based on $\times D$-Markov entropy rate. The signal-to-noise ratio (SNR) is varied by adding white Gaussian noise with a (power-level) SNR of certain dB compared to the signal power of 0 dB, which is a significantly weaker signal relative to the pressure signal at a stable state of operation. This procedure of noise incorporation realistically simulates the presence of low-level sensor noise. It is observed from Figure 14(a) and (b) that the RR and entropy of the probability distribution of diagonal length, obtained by the RQA method,[16] drop close to zero well within the range of $Re = 10,000$; this would yield false alarm rates of instability for SNR of ~ 30 dB, when the system is actually far from instability. This happens due to the sensitivity of the measure to the threshold for RQA at different noise levels. Figure 14(c) shows that the variance of minimum permutation entropy[14] at the onset (e.g. *Re* in the range of 8000–10,000) of instability is large, making it difficult to put a uniform threshold on this particular measure for early detection. Figure 14(d) presents the proposed measure based on $\times D$-Markov entropy rate and it shows negligible variance across multiple SNRs. The onset of instability can be predicted with a threshold of 0.9 uniformly for all noise levels shown here. The rationale for high robustness of the proposed measure can be attributed to inherent stability of STSA to varying noise.[44]

Summary, conclusions, and future work

This paper proposes a fast nonlinear tool for early detection of the onset of thermo-acoustic instability in combustion systems. The underlying algorithm is built upon the concepts of STSA[17] with generalized *D*-Markov machines.[22,21] An information-theoretic measure of combustion instability, which models the spatio-temporal co-dependence among heterogeneous (e.g. pressure and chemiluminescence) sensors, is constructed to capture the precursors before visible appearance of instability. A series of experiments with different protocols (e.g. varying Reynolds number (*Re*) at constant FFR, varying equivalence ratio Φ at constant AFR) have been conducted on a swirl-stabilized combustor (see ''Description of the experimental apparatus'' section) at different premixing conditions for testing and experimental validation of the proposed method of instability prediction. Real-time modeling of *D*-Markov and $\times$D-Markov machines has been performed on a part of the acquired data to evaluate the corresponding entropy rates of the complete time series.

It is observed that the state complexity of the *D*-Markov machines starts dropping drastically as the instability creeps in. It is also observed that the variations in the $\times D$-Markov entropy rates between farthest sensors are monotonic in nature before the onset of instability for all protocols of the experiment. The proposed measure of instability is found to be robust relative to shorter lengths of time-series data, which would be useful for real-time combustion control. The proposed method has been compared with other state-of-the-art techniques (e.g. minimum permutation entropy,[41] RQA-based measures,[45] and Hurst exponent[9]) for time complexity and performance in terms of early detection of instability precursors. The results of comparison show that the $\times D$-Markov entropy rate-based method is among the fastest in the lot as it can detect the onset of instability early enough with a generic threshold across all protocols. The proposed measure also exhibits robustness to varying level of sensor noise.

While there are many other areas yet to be addressed in this context, a few topics of future research are delineated below.

- Extension of the proposed method of instability prediction to other types of combustors operating under different kinds of protocols.
- More rigorous analysis of intermittence-based route to instability via short-time STSA.[46]
- Design of experiments with varying *Re* or Φ for a better understanding of the transient behavior at the onset of instability.
- Investigation of the behavior of flame oscillations under partially premixed fuel-air inputs to develop stabilization algorithms;
- Development of a systematic approach for analysis of data-driven instability precursors from high-speed images and particle image velocimetry (PIV) data.
- Possible extension to decision and control of combustion instability based on the proposed information-theoretic metrics.

Acknowledgements

The authors thankfully acknowledge the benefits of discussion with Professor Achintya Mukhopadhyay, Mr Devesh K Jha, and Dr Shashi Phoha.

Declaration of conflicting interests

The author(s) declared no potential conflicts of interest with respect to the research, authorship, and/or publication of this article.

Funding

The author(s) disclosed receipt of the following financial support for the research, authorship, and/or publication of this article: The analytical part of the work reported in this paper has been supported in part by the US Air Force Office of Scientific Research (AFOSR) under Grant No. FA9550-15-1-0400, and the experimental part by National Centre for Combustion R & D at Indian Institute of Technology Madras, Chennai, India. Any opinions, findings and conclusions or recommendations expressed in this publication are those of the authors and do not necessarily reflect the views of the sponsoring agencies.

References

1. Lieuwen T, Torres H, Johnson C, et al. A mechanism of combustion instability in lean premixed gas turbine combustors. *J Eng Gas Turb Power* 2000; 123: 182–189.
2. McManus K, Poinsot T and Candel SM. A review of active control of combustion instabilities. *Prog Energy Combust Sci* 1993; 19: 1–29.
3. Dowling AP and Hubbard S. Instability in lean premixed combustors. *J Power Energy* 2000; 214: 317–332.
4. Huang Y and Yang V. Dynamics of stability of lean premixed swirl stabilized combustion. *Prog Energy Combust Sci* 2009; 35: 293–364.
5. Candel S, Durox D, Schuller T, et al. Dynamics of swirling flames. *Ann Rev Fluid Mech* 2014; 46: 147–173.
6. Palies P, Schuller T, Durox D, et al. Modelling of premixed swirling flame transfer functions. *Proc Combust Inst* 2011; 33: 2967–2974.
7. Bellows B, Bobba M, Forte A, et al. Flame transfer function saturation mechanisms in a swirl stabilized combustor. *Proc Combust Inst* 2007; 31: 3181–3188.
8. Noiray N, Durox D, Schuller T, et al. A unified framework for nonlinear combustion instability analysis based on flame describing function. *J Fluid Mech* 2008; 615: 139–167.
9. Nair V and Sujith RI. Multifractality in combustion noise: predicting an impending combustion instability. *J Fluid Mech* 2014; 747: 635–655.

10. Nair V, Thampi G, Karuppusamy S, et al. Loss of chaos in combustion noise as a precursor of impending combustion instability. *Int J Spray Combust Dyn* 2013; 5: 273–290.
11. Chakravarthy SR, Sivakumar R and Shreenivasan OJ. Vortex acoustic lock on in bluff body and backward facing step combustors. *Sadhana* 2007; 32: 145–154.
12. Lieuwen T. Online combustor stability margin assessment using dynamic pressure data. *J Eng Gas Turb Power* 2005; 127: 478–482.
13. Gotoda H, Nikimoto H, Miyano T, et al. Dynamic properties of combustion instability in a lean premixed gas-turbine combustor. *Chaos* 2011; 21: 013124.
14. Gotoda H, Amano M, Ikawa T, et al. Characterization of complexities in combustion instability in a lean premixed gas-turbine model combustor. *Chaos* 2012; 22: 043128.
15. Murugesan M and Sujith R. Combustion noise is scale-free: transition from scale-free to order at the onset of thermoacoustic instability. *J Fluid Mech* 2015; 772: 225–245.
16. Nair V, Thampi G and Sujith R. Intermittency route to thermoacoustic instability in turbulent combustors. *J Fluid Mech* 2014; 756: 470–487.
17. Daw C, Finney C and Tracy E. A review of symbolic analysis of experimental data. *Rev Sci Instrum* 2003; 74: 915–930.
18. Daw C, Kennel M, Finney C, et al. Observing and modeling nonlinear dynamics in an internal combustion engine. *Phys Rev E* 1998; 57: 2811–2819.
19. Mukhopadhyay A, Chaudhuri R, Paul T, et al. Prediction of lean blow-out in gas turbine combustors using symbolic time series analysis. *J Propul Power (AIAA)* 2013; 29: 950–960.
20. Unni V, Mukhopadhyay A and Sujith R. Online detection of impending instability in a combustion system using tools from symbolic time series analysis. *Int J Spray Combust Dyn* 2015; 7: 243–255.
21. Mukherjee K and Ray A. State splitting and state merging in probabilistic finite state automata for signal representation and analysis. *Signal Process* 2014; 104: 105–119.
22. Ray A. Symbolic dynamic analysis of complex systems for anomaly detection. *Signal Process* 2004; 84: 1115–1130.
23. Rajagopalan V and Ray A. Symbolic time series analysis via wavelet-based partitioning. *Signal Process* 2006; 86: 3309–3320.
24. Subbu A and Ray A. Space partitioning via Hilbert transform for symbolic time series analysis. *Appl Phys Lett* 2008; 92: 084 107–1 to 084 107–3.
25. Ramanan V, Chakravarthy SR, Sarkar S, et al. Investigation of combustion instability in a swirl-stabilized combustor using symbolic time series analysis. In: *Proceeding of ASME gas turbine India conference, GTIndia 2014*, New Delhi, India, December 2014, pp.1–6.
26. Sarkar S, Ray A, Mukhopadhyay A, et al. Dynamic data-driven prediction of lean blowout in a swirl-stabilized combustor. *Int J Spray Combust Dyn* 2015; 7: 209–242.
27. Darema F. Dynamic data driven applications systems: new capabilities for application simulations and measurements. In: *5th international conference on computational science—ICCS 2005*, Atlanta, GA, 2005, pp.610–615.
28. Sarkar S, Sarkar S, Virani N, et al. Sensor fusion for fault detection and classification in distributed physical processes. *Front Robot AI* 2014; 1: 16.
29. Cover T and Thomas J. *Elements of information theory*, 2nd ed. Hoboken, NJ: Wiley, 2006.
30. Lind D and Marcus B. *Symbolic dynamics and coding*. Cambridge, UK: Cambridge University Press, 1995.
31. Dupont P, Denis F and Esposito Y. Links between probabilistic automata and hidden Markov models: probability distributions, learning models and induction algorithms. *Pattern Recogn* 2005; 38: 1349–1371.
32. Vidal E, Thollard F, de la Higuera C, et al. Probabilistic finite-state machines—Part I and Part II. *IEEE Trans Pattern Anal Mach Intell* 2005; 27: 1013–1039.
33. Rao C, Ray A, Sarkar S, et al. Review and comparative evaluation of symbolic dynamic filtering for detection of anomaly patterns. *Signal Image Video Process* 2009; 3: 101–114.
34. Bahrampour S, Ray A, Sarkar S, et al. Performance comparison of feature extraction algorithms for target detection and classification. *Pattern Recogn Lett* 2013; 34: 2126–2134.
35. Bishop CM. *Pattern recognition and machine learning*. New York, NY: Springer, 2006.
36. Sipser M. *Introduction to the theory of computation*, 3rd ed. Boston, MA: Cengage Publishing, 2013.
37. Sarkar S, Jha D, Lore K, et al. Multimodal spatiotemporal information fusion using neural-symbolic modeling for early detection of combustion instabilities. In: *Preprints American control conference,* Boston, MA, July 2016.
38. Jha D, Srivastav A, Mukherjee K, et al. Depth estimation in Markov models of time-series data via spectral analysis. In: *2015 American control conference*, Chicago, IL, July 2015, pp.5812–5817.
39. Abarbanel H. *Analysis of observed chaotic data*. New York, NY: Springer-Verlag, 1996.
40. Sarkar S, Chattopadhyay P, Ray A, et al. Alphabet size selection for symbolization of dynamic data-driven systems: an information-theoretic approach. In: *American control conference,* Chicago, IL, June–July 2015, pp.5194–5199.
41. Bandt C and Pompe B. Permutation entropy: a natural complexity measure for time series. *Phys Rev Lett* 2002; 88: 174102.

42. Unni V and Sujith R. Multifractal characteristics of combustor dynamics close to lean blowout. *J Fluid Mech* 2015; 784: 30–50.
43. Unakafova V and Keller K. Efficiently measuring complexity on the basis of real-world data. *Entropy* 2013; 15: 4392–4415.
44. Sarkar S, Jin X and Ray A. Data-driven fault detection in aircraft engines with noisy sensor measurements. *J Eng Gas Turb Power* 2011; 133: 081602.
45. Kabiraj L and Sujith R. Nonlinear self-excited thermoacoustic oscillations: intermittency and flame blowout. *J Fluid Mech* 2012; 713: 376–397.
46. Sarkar S, Mukherjee K, Sarkar S, et al. Symbolic dynamic analysis of transient time series for fault detection in gas turbine engines. *J Dyn Syst Meas Control* 2013; 135: 014506.